Dalton Transactions

PAPER

Cite this: *Dalton Trans.*, 2018, **47**, 15907

A versatile chemosensor for the detection of Al^{3+} and picric acid (PA) in aqueous solution†

Barnali Naskar,[a] Antonio Bauzá,[b] Antonio Frontera,[b] Dilip K. Maiti,[a] Chitrangada Das Mukhopadhyay[c] and Sanchita Goswami *[a]

Received 4th June 2018,
Accepted 10th October 2018

DOI: 10.1039/c8dt02289e

rsc.li/dalton

Developing chemosensors for efficient detection of Al^{3+} and picric acid in water is in high demand but challenging. In this paper, we have demonstrated the potential of a probe, 6,6′-(1*E*,1′*E*)-(2-hydroxypropane-1,3-diyl)bis(azan-1-yl-1-ylidene)bis(methan-1-yl-1-ylidene)bis(2-methoxyphenol) (**H_2Vm**), as a "switch-on" Al^{3+} responsive fluorescence chemosensor in water. In addition to the ability of **H_2Vm** to sense Al^{3+}, the **Al_2-Vm_2** complex offers selectivity towards picric acid (PA) in HEPES buffer (pH = 7.4) solution (detection limit (20.13×10^{-9} M) *via* "switch-off" mode. The reversible fluorescence response with low detection limit (11.34×10^{-9} M) in the pH range of 6.0–9.0 makes **H_2Vm** suitable for tracking Al^{3+} in live HCT cells. The resulting **Al_2-Vm_2** complex is also responsive towards PA in HCT cells. Thus, a versatile fluorescence spectroscopy-based chemosensor for Al^{3+} and picric acid has been developed with possible applications in human health and national security.

1. Introduction

Recent research has demonstrated great potential in chemosensors based on fluorescence spectroscopy as they provide a fascinating platform for simple, selective, sensitive, portable and real-time detection of physiologically and environmentally relevant analytes.[1] Aluminium is the third most abundant element on earth and is used rigorously in the pharmaceutical sector, cosmetics, manufacturing and packaging industries, which leads to easy accumulation in the human body.[2] Physiological conditions associated with abnormal levels of Al^{3+} include Alzheimer's and Parkinson's disease and degeneration of the nervous system.[3] Traditionally, there are a couple of analytical techniques available for detecting Al^{3+} ions, including atomic absorption spectroscopy[4] and inductively-coupled plasma mass spectrometry.[5] However, these methods suffer from disadvantages such as time-consuming sample preparation, expensive equipment, and nonportability, which limit their applications. In this context, the use of fluorescence spectroscopy-based chemosensors enables highly selective and sensitive real time monitoring of Al^{3+} ions in living cells. The World Health Organization (WHO) prescribed the human intake of aluminium as 3–10 mg per day, with a weekly dietary intake of 7 mg per day.[6] Compared with transition metals, the detection of Al^{3+} poses a challenge due to its lack of spectroscopic characteristics and poor coordination ability.[7a] Though a number of Al^{3+} sensors have been reported in the literature,[7b] it is always desirable to fabricate highly selective, sensitive, efficient and convenient chemosensors for Al^{3+} in water. The development of suitable chemosensors for the rapid and selective detection of chemical explosives at trace levels has received increasing attention in the fields of forensic analysis and criminal investigations.[8] Picric acid (PA) is a well-known highly energetic chemical substance of explosive nature.[9] PA is widely used in rocket fuel manufacturing, as an antiseptic agent and as a yellow pigment in leather industries.[10] Since it shows high solubility in water (14 g L^{-1} at 20 °C), PA and its derivatives are deemed environmentally hazardous and represent a major threat to ground water contamination.[11] According to WHO,[12] the allowed concentration of PA in ground water is 0.001 mg L^{-1} Moreover, exposure to PA is linked to eye irritation, headache, anaemia, kidney problems and severe liver and respiratory organ damage.[13] Therefore, the development of selective and highly sensitive sensors for PA is of great importance.[14] A number of techniques such as ion-mobility spectrometry (IMS),[15a] surface-enhanced Raman spectroscopy (SERS),[15b] and gas chromatography (GC)[15c] are available for the detection of PA.[15] However, high cost, lack of portability, and low selectivity restrict their practical applicability. In contrast, fluorescent chemosensors are an effective tool for PA detection.[16]

[a]*Department of Chemistry, University of Calcutta, 92, A.P.C. Road, Kolkata, India. E-mail: sgchem@caluniv.ac.in*
[b]*Departament de Química, Universitat de les IllesBalears, Crta. deValldemossa km 7.5, 07122 Palma de Mallorca, Baleares, Spain*
[c]*Centre for Healthcare Science & Technology, Indian Institute of Engineering Science and Technology, Shibpur, Howrah 711103, India*

†Electronic supplementary information (ESI) available: NMR spectrum, FT-IR, ESI-MS spectrum, photophysical characterization, theoretical data, cell viability. See DOI: 10.1039/c8dt02289e

Presently, a crucial issue related to the chemosensors is related to solvents as many solvents decrease the accessibility of the probe in the living cells, leading to compromised performance.[17] From a practical point of view, the detection of Al^{3+}/PA in aqueous medium is highly desirable.

Herein, a Schiff base probe, 6,6′-(1*E*,1′*E*)-(2-hydroxypropane-1,3-diyl)bis(azan-1-yl-1-ylidene)bis(methan-1-yl-1-ylidene)bis(2-methoxyphenol) (**H_2Vm**) has been synthesized by condensation of *o*-vanillin and 1,3-diamino-2-hydroxypropane in methanol solution, as reported in previous literature reports.[18] **H_2Vm** works as an efficient sensor for the visual and rapid detection of Al^{3+} in water. In addition, the detection of the explosive picric acid can be realized in aqueous medium by the resulting probe-Al^{3+} ensemble in the 10^{-9} (M) range. ^{1}H-NMR and ^{13}C-NMR studies and DFT/TDDFT calculations have been performed to elucidate the compositions of the **Al_2-Vm_2** and (**Al_2-Vm_2**)-picric acid ensembles. Cell imaging studies on live HCT cells also established the potential of the probe **H_2Vm**.

2. Experimental section

2.1. General information

o-Vanillin, 1,3-diamino-2-hydroxypropane and HEPES buffer were purchased from Sigma-Aldrich. $Al(NO_3)_3{\cdot}9H_2O$ and other reagents were procured from LOBA and Merck India, respectively. The buffer was prepared using triple distilled water. Solvents used for the spectroscopic studies and for the syntheses were purchased from commercial sources and used as received. Elemental analyses for C, H and N were performed on a Perkin-Elmer 2400 II analyzer. The FT-IR spectra were recorded from KBr pellets in the range of 400–4000 cm^{-1} on a Perkin-Elmer Spectrum 100 spectrometer. ^{1}H- and ^{13}C-NMR spectra were recorded in d_6-DMSO with TMS as the internal standard on a Bruker, AV 300 Supercon Digital NMR system. ESI-MS were recorded on a Qtof Micro YA263 mass spectrometer. A Systronics digital pH meter (model 335) was used to measure the pH of the solution, and the adjustment of pH was conducted using either 50 mM HCl or 50 mM NaOH solution. The absorption and emission spectra were recorded on a Hitachi UV–Vis U-3501 spectrophotometer and Perkin-Elmer LS55 fluorimeter, respectively. Time-resolved fluorescence lifetime measurements were performed on a HoribaJobinYvonFluorocube-01-NL time-correlated single photon counting (TCSPC) set up employing a picosecond delta diode (DD-375L) operating at λ_{ex} = 375 nm and a repetition rate of 1 MHz as the excitation source. The overall temporal and spectral resolution of the instrument were both ~60 ps. Average fluorescence lifetimes (τ_{avg}) were calculated from the decay times and pre-exponential factors using the following equation:

$$\tau_{avg} = \frac{\sum \alpha_i \tau_i^2}{\sum \alpha_i \tau_i}$$

where α_i is the pre-exponential factor corresponding to the i^{th} decay time constant, τ_i.

Fluorescence quantum yield was determined using quinine sulphate (Φ_R = 0.546 in 0.1 M H_2SO_4) as the standard in methanol solution. The quantum yield was calculated using the following equation:

$$\phi_s = \phi_R \frac{A_s}{A_R} \times \frac{Abs_R}{Abs_S} \times \frac{{\eta_S}^2}{{\eta_R}^2}$$

where the *A* terms denote the integrated area under the fluorescence curve, Abs denotes absorbance, η is the refractive index of the medium and ϕ is the fluorescence quantum yield. Subscripts S and R denote the respective parameters for the studied sample and reference, respectively.

2.2. Theoretical methods

The compounds were initially optimized at the PB86-D3/def2-TZVP level of theory in their singlet ground state (S_0). We performed the time-dependent DFT (TDDFT)[19] calculations using the B3LYP/6-311+G* level of theory associated with the conductor-like polarizable continuum model (CPCM).[20,21] The B3LYP functional is more reliable than PB86 for reproducing the experimental UV spectra in the metal complexes studied herein. For the complexes and ligands (keto and enol forms), we calculated 60 singlet–singlet transitions using their ground S_0 state geometries and using the conductor-like polarizable continuum model. For all atoms, we used 6-311+G* as the basis set. The calculated electronic density plots for the frontier molecular orbitals were prepared using the GaussView 5.0 software. All the calculations were performed using the Gaussian 09 software package.[22]

2.3. Synthesis and characterisation

Synthesis of the ligand (H$_2$Vm). *o*-Vanillin (0.304 g, 2.0 mmol) was dissolved in methanol (15 mL). To this solution, a solution of 1,3-diamino-2-hydroxypropane (0.090 g, 1.0 mmol), also dissolved in the same solvent (15 mL), was added dropwise at room temperature. The reaction mixture was then heated under reflux for 6 h and allowed to cool to room temperature. A yellow solid product (**H_2Vm**) was obtained by evaporation of the solvent in a rotary evaporator. (Yield: 95%) Anal. Calcd for $C_{19}H_{22}N_2O_5$: C, 63.67; H, 6.19; N, 7.82; found: C, 63.66; H, 6.18; N, 7.81; ^{1}H NMR (300 MHz, d_6-DMSO) δ H: 13.66 (s, 2H, –OH), 8.41 (s, 2H, CH═N), 6.94–6.91 (m, 4H, ArH), 6.72–6.66 (m, 2H, ArH), 5.16 (s, 1H, –OH), 3.92 (s, 1H, CH), 3.68 (s, 6H, –OCH_3), 3.54–3.44 (m, 4H, CH_2); ^{13}C NMR (300 MHz, d_6-DMSO) δ C: 166.7, 151.8, 147.7, 122.8, 117.8, 117.0, 114.2, 68.8, 61.5, 55.3 (Fig. S1†). Selected FT-IR data (KBr, cm^{-1}), (Fig. S2†) $\nu_{(O-H)}$ = 3433.59 cm^{-1}, $\nu_{(C=N)}$ = 1636.04 cm^{-1}, ESI-MS *m*/*z*, ion: 359.1583, [**H2Vm** + H]$^+$, 381.1414, [**H2Vm** + Na]$^+$ (Fig. S3†).

Synthesis of Al_2-Vm_2 complex (1). A methanol solution (5 mL) of $Al(NO_3)_3{\cdot}9H_2O$ (0.626 g, 2 mmol) was mixed under stirring with the solution (5 mL) of the ligand **H_2Vm** (0.358 g, 1.0 mmol) in the same solvent. The mixture was continuously stirred for 2 h and the resulting clear solution was

allowed to evaporate slowly at room temperature for one week, yielding a yellow crystalline compound which were collected by filtration, washed with methanol and ether successively, and dried in air (Yield: 79%). Anal. Calcd for $C_{38}H_{40}N_6O_{16}Al_2$: C, 51.24; H, 4.53; N, 9.44; found: C, 51.23; H, 4.52; N, 9.45. Selected FT-IR data (KBr, cm^{-1}) (Fig. S2†) $\nu_{(OH)}$ = 3432 cm^{-1}, $\nu_{(C=N)}$ = 1632 cm^{-1}, $\nu_{nitrate}$ = 1470 cm^{-1}, ESI-MS *m*/*z*, ion: 383.1162, $[(HVm)_2 + (Al)_2]^{2+}$, (Fig. S3†).

Synthesis of Al_2-Vm_2·PA complex (2). To a solution of the **Al_2-Vm_2** complex (**1**) in methanol (0.890 g, 1.0 mmol), PA (picric acid) (0.458 g, 2.0 mmol) was added dropwise and then, the reaction mixture was stirred for 4.0 h at room temperature. Then, this solution was filtered. The pure recrystallized product, comprising single crystals suitable for the X-ray crystallographic study, was isolated from the methanol solution by slow evaporation (Yield: 81%). Anal. Calcd for $C_{50}H_{44}N_{10}O_{24}Al_2$: C, 49.11; H, 3.63; N, 11.45; found: C, 49.12; H, 3.62; N, 11.46. Selected FT-IR data (KBr, cm^{-1}): $\nu_{(C=N)}$ = 1631.76 cm^{-1}, (Fig. S2†). ESI-MS *m*/*z* ion: 1223.2205, $[(Vm)_2 + (Al)_2 + 2PA + H]^+$ (Fig. S3†).

2.4. Cell study of H_2Vm

Materials methods. Frozen human colorectal carcinoma cell line **HCT 116** and **HeLa** cells were obtained from NCCS, Pune, India and maintained in Dulbecco's modified Eagle's medium (DMEM, Sigma Chemical Co., St Louis, MO, USA) supplemented with 10% fetal bovine serum (Invitrogen), penicillin (100 μg mL^{-1}), and streptomycin (100 μg mL^{-1}). The cells were initially propagated in a 25 cm^2 tissue culture flask in an atmosphere of 5% CO_2 and 95% air at 37 °C humidified air till 70–80% confluency.

Fluorescent imaging studies. For fluorescence imaging studies, 1×10^{-5} cells of **HCT 116** in 150 μL media were seeded on a sterile 12 mm diameter poly-L-lysine-coated coverslip and kept in a sterile 35 mm covered petri dish and incubated at 37 °C in a CO_2 incubator for 24–30 h. Next day, the cells were washed three times with phosphate buffered saline (pH 7.4) and fixed using 4% paraformaldehyde in PBS (pH 7.4) for 10 minutes at room temperature. Then, the cells were washed with PBS, followed by permeabilization using 0.1% saponin for 10 minutes. Then, the cells were incubated with 2.0×10^{-4} M $Al(NO_3)_3·9H_2O$ dissolved in 100 μL DMEM at 37 °C for 1 h in a CO_2 incubator and observed under an epifluorescence microscope (Carl Zeiss). The cells were again washed thrice with PBS (pH 7.4) to remove any free metal and incubated in DMEM containing **H_2Vm** probe to a final concentration of 1×10^{-6} M, followed by washing with PBS (pH 7.4) three times to remove excess probe outside the cells. Again, images were taken using an epifluorescence microscope. In a separate coverslip undergoing the same treatment, the cells were treated with the probe alone without any aluminium salt. Before fluorescence imaging, all the solutions were aspirated out and mounted on slides in a mounting medium containing DAPI (1 μg mL^{-1}) and stored in the dark before the microscopic images were acquired.

Cytotoxicity assay. The cytotoxic effects of the probe, $Al(NO_3)_3·9H_2O$ and the **Al_2-Vm_2** complex were determined by an MTT assay following the manufacturer's instructions (MTT 2003, Sigma-Aldrich, MO). HCT cells were cultured into 96-well plates (approximately 10^4 cells per well) for 24 h. Next day, the media was removed and various concentrations of the probe, $Al(NO_3)_3·9H_2O$ and the **Al_2-Vm_2** complex (0, 20, 30, 50, 75, and 100 μM) were added to the cells and incubated for 24 h. Control samples with no cells and cells in DMEM without any treatment were also included in the study. Following incubation, the growth media were removed, and fresh DMEM containing MTT solution was added. The plate was incubated for 3–4 h at 37 °C. Subsequently, the supernatant was removed, the insoluble colored formazan product was solubilized in DMSO, and its absorbance was measured in a microtiter plate reader (PerkinElmer) at 570 nm. The assay was performed in triplicate for each concentration of the probe, $Al(NO_3)_3·9H_2O$ and the **Al_2-Vm_2** complex. The OD value of the wells containing only the DMEM medium was subtracted from all readings to get rid of the background influence. The data analysis and calculation of standard deviation was performed using Microsoft Excel 2007 (Microsoft Corporation).

3. Results and discussion

3.1. Syntheses and general characterization

H_2Vm was synthesized *via* a one-step simple condensation reaction between *o*-vanillin and 1,3-diamino-2-hydroxypropane in methanol solution (Scheme 1). The formation of the probe was fully characterized by various spectroscopic techniques such as ^{1}H- and ^{13}C-NMR spectroscopy, FT-IR spectroscopy, CHN analysis, and ESI-MS spectrometry (Fig. S1, S2, S3†).

From the Job's plot analysis, the results indicate 1 : 1 binding stoichiometry between **H_2Vm** and Al^{3+} (Fig. S7†). In the ESI-MS spectra of **H_2Vm**, a peak at *m*/*z* 359.1583 and 381.1414 are assigned to [**H2Vm** + H]$^+$ and [**H2Vm** + Na]$^+$,

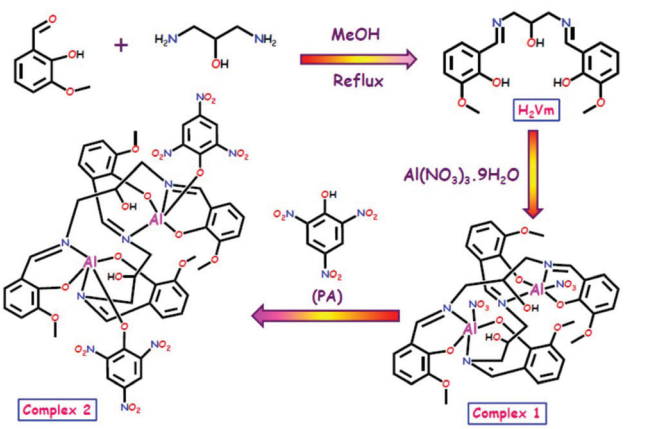

Scheme 1 Schematic of the synthesis of the ligand (H_2Vm) in complexes **1** and **2**.

respectively (Fig. S3†). The ESI-MS study of the **Al_2-Vm_2** complex (**1**) depicts a doubly charged ion peak at m/z = 383.1162, which is assignable to $[(HVm)_2 + (Al)_2]^{2+}$. The mass spectrum of the **Al_2-Vm_2** complex with picric acid (**2**) shows a peak at m/z = 1223.2205 corresponding to $[(Vm)_2 + (Al)_2 + 2PA + H]^+$ (Fig. S3†).

3.2. Photophysical characteristics of H_2Vm and the Al_2-Vm_2 ensemble

The photophysical properties of **H_2Vm** were studied in HEPES buffer (pH = 7.4) solution. The UV-Vis absorption spectrum of **H_2Vm** exhibited a broad band at 420 nm at room temperature. Upon addition of Al^{3+} solution ((0.5–5.0) × 10^{-7} M) to **H_2Vm** (5 × 10^{-7} M), the absorption band at 420 nm gradually decreased, and a new absorption band appeared at 368 nm with a concomitant increase in intensity; also, two well-defined isosbestic points appeared at 340 nm and 398 nm (Fig. 1, Fig. S8 and S9†). Interestingly, the addition of Al^{3+} to the solution of **H_2Vm** produced a colour change from yellow to colourless, whereas other metal ions, such as Li^+, Na^+, K^+, Ca^{2+}, Mg^{2+}, Mn^{2+}, Ba^{2+}, Cu^{2+}, Ni^{2+}, Co^{2+}, Fe^{2+}, Fe^{3+}, Zn^{2+}, Cd^{2+}, Hg^{2+}, Pb^{2+}, Sr^{2+} and Cr^{3+}, absorbed very weakly in this region (Fig. S10†). Thus, an instrument-free, direct and visual detection method is available with a detection limit of 11.34 × 10^{-9} (M). The study of the binding stoichiometry using Job's plot indicated a 1 : 1 association between **H_2Vm** and Al^{3+} (Fig. S7†). The binding constant of **H_2Vm** with Al^{3+} was determined to be 5.23 × 10^5 M^{-1} by UV-Vis titration[23] (Fig. S11†).

The emission spectra of the free chemosensor **H_2Vm** were recorded upon excitation at 368 nm, 400 nm and 450 nm. They exhibited very weak fluorescence emission at 488 nm (Φ = 0.036) in HEPES buffer (pH = 7.4) solution (Fig. S12 and S13†). In contrast, a portion-wise addition of Al^{3+} (0.5–5.0) × 10^{-7} M to an aqueous solution of **H_2Vm** elicited significant fluorescence enhancement (Φ = 0.511) in the emission profile at 488 nm (Fig. 2, Fig. S14, S15, S16 and S17†). We then screened the probe **H_2Vm** against a series of cations and interestingly, only Al^{3+} could induce an enhancement in the fluorescence at 488 nm, while other cations did not produce significant fluorescence changes. We then introduced the same concentrations of other relevant metal ions, such as Li^+, Na^+, K^+, Ca^{2+}, Mg^{2+}, Mn^{2+}, Ba^{2+}, Cu^{2+}, Ni^{2+}, Co^{2+}, Fe^{2+}, Fe^{3+}, Zn^{2+}, Cd^{2+}, Hg^{2+}, Pb^{2+}, Sr^{2+} and Cr^{3+} to evaluate competitive binding interactions. The results are depicted in Fig. 3 and Fig. S18.† Therefore, **H_2Vm** offers a selective fluorescence "turn-on" sensing of Al^{3+}. The probe **H_2Vm** is selective towards Al^{3+} probably because of the intrinsic physical features of Al^{3+}, which are high charge (+3) and small ionic radius (the smallest of the series). The emission responses were analyzed by fitting the data of the fluorescence titration experiment of **H_2Vm** with Al^{3+} to the Benesi–Hildebrand equation, and the association constant for **Al_2-Vm_2** was determined to be 4.19 × 10^5 M^{-1}

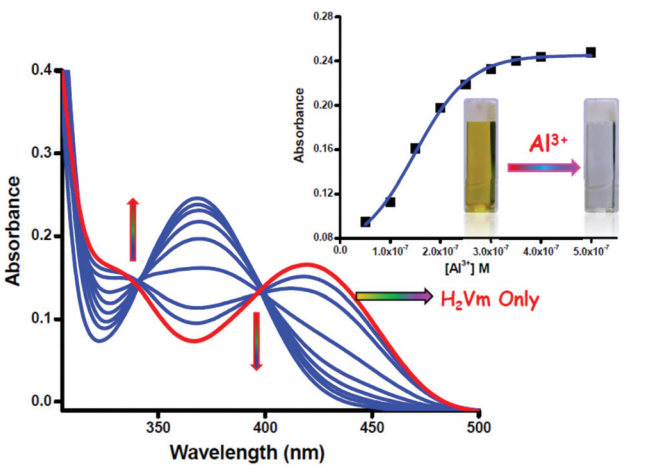

Fig. 1 UV-vis spectra of **H_2Vm** (5 × 10^{-7} M) in a HEPES buffer (pH = 7.4) solution in the presence of various concentrations of Al^{3+} (0, 0.5, 1, 1.5, 2, 2.5, 3, 4 and 5) × 10^{-7} M. Inset: Absorbance of **H_2Vm** at 368 nm as a function of $[Al^{3+}]$.

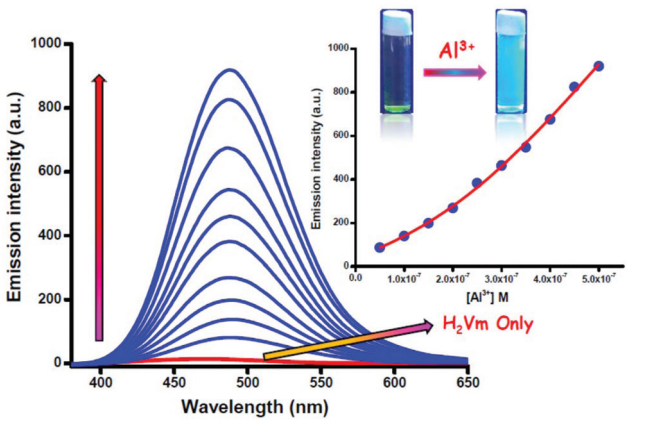

Fig. 2 Emission spectra of **H_2Vm** (5 × 10^{-7} M) in the presence of an increasing amount of $[Al^{3+}]$ (0, 0.5, 1, 1.5, 2, 2.5, 3, 3.5, 4, 4.5 and (5 × 10^{-7} M) in a HEPES buffer (pH = 7.4) solution (λ_{ex} = 368 nm, λ_{em} = 488 nm). Inset: Fluorescence emission intensity of **H_2Vm** at 488 nm as a function of $[Al^{3+}]$.

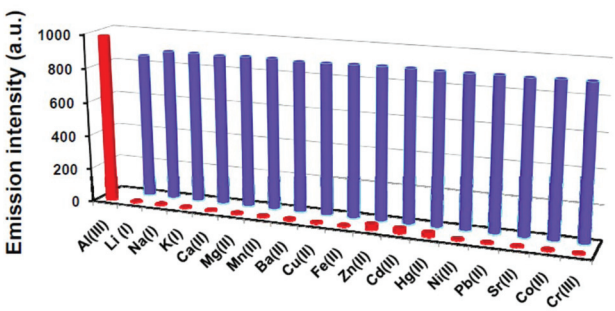

Fig. 3 Variation of the fluorescence intensity of **H_2Vm** (5 × 10^{-7} M) in the presence of 2 equiv. of different cations except 1.0 equiv. of Al^{3+} in solution [the red bar portion]. Fluorescence intensity of a mixture of **H_2Vm** (5 × 10^{-7} M) with other metal ions followed by addition of Al^{3+} to the HEPES buffer (pH = 7.4) solution [the blue bar portion] (λ_{ex} = 368 nm, λ_{em} = 488 nm).

(Fig. S19†). We calculated the stability constant values for the **H_2Vm**-metal ion ensemble for all the metal ions listed above (Table S3†). It was observed that the **H_2Vm**-Al^{3+} complex bears the highest stability constant value, which explains its selectivity.

The detection limit for Al^{3+} was calculated to be 11.34×10^{-9} (M) on the basis of $3\sigma/S$ (Fig. S20†), which is much lower than the limit specified by WHO.[24] Therefore, **H_2Vm** could act as an effective sensor for the detection of Al^{3+} in drinking water. The fluorescence enhancement is achieved, presumably due to the increased rigidity of the resulting system upon chelation, preventing the possibility of intramolecular rotation, leading to nonradiative decay. Reversibility of the sensing process was established by the alternating addition of Al^{3+}/Na_2H_2EDTA (Fig. S21†).

Furthermore, fluorescence lifetime measurements were recorded further to understand the mechanism of the switch-on sensor response of **H_2Vm** toward an Al^{3+} ion as shown in Fig. S22.† According to the equations $\tau^{-1} = k_r + k_{nr}$ and $k_r = \Phi_f/\tau$, the radiative decay rate constant k_r and the total non-radiative decay rate constant k_{nr} of **H_2Vm** and Al^{3+}-bound species were calculated (Table S2†). The data indicate that fluorescence enhancement occurs due to the decrease in the ratio of k_{nr}/k_r from 26.81 for **H_2Vm** to 0.957 for **Al_2-Vm_2**, which is in agreement with the chelation-enhanced fluorescence (CHEF) process.

The fluorescence spectral nature of **H_2Vm** was investigated without and with Al^{3+} as a function of pH (from 2.0 to 12.0) in aqueous solution at 488 nm. As shown in Fig. S23,† it can be clearly observed that the emission intensity of **H_2Vm** is negligible throughout the pH range, whereas the emission intensity of the **Al_2-Vm_2** ensemble reached a maximum in the pH 6.0–9.0 region. In the acidic zone (pH < 6.0), dissociation of the complex due to protonation decreases the emission intensity. At higher pH values (pH > 9.0), OH^- ions provide competition to **H_2Vm** for Al^{3+}, causing aluminium hydroxide precipitation, and thus lowering the emission intensity.

3.3. NMR titration and composition of an Al_2-Vm_2 aggregate

The response mechanism of **H_2Vm** for Al^{3+} was further investigated by means of ^{1}H- and ^{13}C-NMR titrations in DMSO-d_6 solution upon the addition of different concentrations of $Al(NO_3)_3 \cdot 9H_2O$ (Fig. S4, S5 and Table S1†). The addition of 0.5 equiv. Al^{3+} to a solution of **H_2Vm** resulted in the complete disappearance of the proton H_a. On gradual addition of 2.0 equiv. Al^{3+}, it was found that the proton peak H_b at 8.412 ppm was shifted downfield to 10.176 ppm due to the coordination of **H_2Vm** with the Al^{3+} ions. The ^{13}C-NMR spectrum of **H_2Vm** revealed signals at 151.83 and 166.73 ppm for the C_a and C_b fragments, respectively. On addition of 2.0 equiv. Al^{3+} to the **H_2Vm** solution, both C_a and C_b carbon signals were downfield-shifted by 17.26 and 24.94 ppm, respectively. The changes in the ^{13}C-NMR symbolic peaks indicate the formation of a strong coordination of Al^{3+} to **H_2Vm**.

3.4. Response of the Al_2-Vm_2 ensemble towards picric acid (PA)

We then set out to assess the highly fluorescent **Al_2-Vm_2** ensemble against organic nitro derivative explosives such as picric acid (PA), 2-nitrotoluene (2-NT), and 2-nitrophenol (2-NP) (Fig. 4). Interestingly, PA induced selective quenching of the fluorescence intensity (Φ = 0.095) of the ensemble in HEPES buffer (pH = 7.4) solution, while the other analytes did not produce significant changes (Fig. 5). As mentioned earlier, the UV-Vis absorption spectrum of the **Al_2-Vm_2** complex is characterized by a well-defined peak at 368 nm at room temperature. The addition of PA to the solution of the **Al_2-Vm_2** complex in a HEPES buffer (pH = 7.4) solution generates a peak at 352 nm along with isosbestic points at 306 nm and 280 nm, indicating the interaction between the **Al_2-Vm_2** complex and PA (Fig. S24†). The detection limit of the **Al_2-Vm_2** complex toward PA was calculated to be 20.13×10^{-9} (M) according to the equation LOD = $K\sigma/S$, where K = 3, σ denotes the standard deviation of the blank solution and S denotes the slope of the calibration curve (Fig. S25†).

The Job's plot pointed towards a 1 : 2 binding stoichiometry between the **Al_2-Vm_2** complex and PA (Fig. S26†). Therefore, we

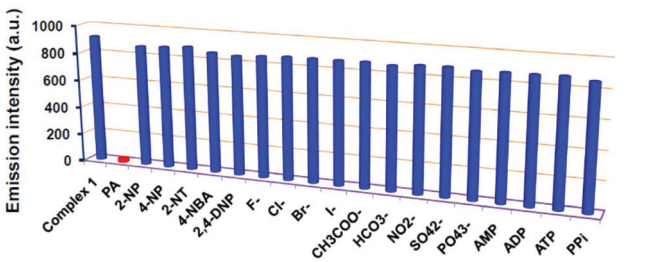

Fig. 4 Variation of the fluorescence intensity of the [**Al_2-Vm_2**] complex (**1**) [(5×10^{-7} M), the cyan bar portion] in the presence of 2.0 equiv. **PA** [the red bar portion] and 4.0 equiv. of different anions [the blue bar portion] in the HEPES buffer (pH = 7.4) solution.

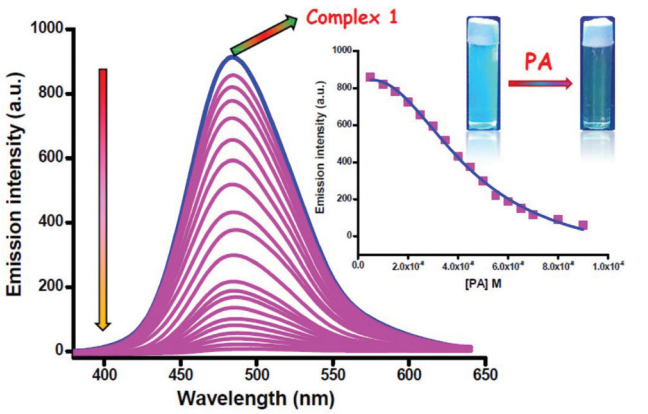

Fig. 5 Emission spectra of the [**Al_2-Vm_2**] complex (**1**) (5×10^{-7} M) upon a gradual increase in the concentration of **PA** (0, 0.5, 1, 1.5, 2, 2.5, 3, 3.5, 4, 4.5, 5, 5.5, 6, 6.5, 7, 7.5, 8, 8.5, 9, 9.5 and 10×10^{-7}) M in a HEPES buffer (pH = 7.4) solution (λ_{ex} = 365 nm, λ_{em} = 484 nm). Inset: Fluorescence emission intensity changes for the titration of the [**Al_2-Vm_2**] complex (**1**) with **PA** and the visual color change observed with the addition of **PA** to the [**Al_2-Vm_2**] complex (**1**) solution as seen under UV light (λ = 365 nm).

may presume that each aluminium center of the structurally symmetrical **Al_2-Vm_2** complex (*vide infra*) interacts with one picric acid (Scheme 1). The fluorescence quenching data were analyzed using the Stern–Volmer (S–V) equation:

$$(F_0/F) = K_{sv}\,[A] + 1$$

where F_0 is the initial fluorescence intensity of the **Al_2-Vm_2** complex before the addition of the analyte, F is the fluorescence intensity of the **Al_2-Vm_2** complex in the presence of picric acid (PA), [A] is the molar concentration of picric acid (PA), and K_{sv} is the quenching constant (unit: M^{-1}). The value of K_{sv} for the **Al_2-Vm_2** complex was calculated from the linear nature of the plot and found to be $1.165 \times 10^6\ M^{-1}$ (Fig. S27†). Furthermore, time-resolved fluorescence quenching experiments were performed to distinguish between static and dynamic quenching processes, and the unaltered average excited state lifetime value reveals that a static quenching pathway is effective[25] (Fig. S28 and Table S2†). This is further verified by an ESI-MS spectral signature that corresponds to the $[(Vm)_2 + (Al)_2 + 2PA + H]^+$ (Fig. S3†). The interaction between the **Al_2-Vm_2** ensemble and PA in solution was further studied by ^{1}H-NMR titration experiments (Fig. S6†).

3.5. Computational studies of the chemosensor (H_2Vm), Al_2-Vm_2 complex and Al_2-Vm_2 complex with picric acid

The UV-vis absorption spectrum of the ligand was studied at room temperature in MeOH. Experimentally, the **H_2Vm** ligand shows one peak above 400 nm (420 nm). The absorption energy associated with the oscillator strength, the main configurations and the assignments calculated using the TDDFT method (S_0 geometry) for the ligand were studied for the three possible tautomeric forms (Scheme 2). The experimental UV spectrum of the ligand is likely composed of the absorption bands of the bis-keto form at room temperature because this tautomer is the most stable (3.3 kcal mol^{-1} more stable than the keto–enol form). Therefore, only the TD-DFT study of the bis-keto form is further described herein. Moreover, the lowest lying absorption band computed for the bis-keto tautomer (λ = 412 nm) is in reasonable agreement with the experimentally determined absorption band (λ_{exp} = 420 nm).

3.6. Keto form of the probe (H_2Vm)

In the ground state, the HOMO is basically composed of the six-membered keto rings, the conjugated exocyclic C=C bonds, the lone pairs of the sp^3-nitrogen atoms and the oxygen atoms of both keto groups. HOMO−1 is stabilized by only 0.033 eV compared with HOMO. Similarly, the LUMO is basically composed of the six-membered keto rings, the exocyclic C=C bonds, the lone pair of the sp^3-nitrogen atoms and the oxygen atoms of the keto groups. The energy difference between the HOMO and LUMO is 3.413 eV. The calculated lowest lying absorption band is located at 412 nm for the bis-keto form of the ligand (Fig. 6 and Table S4†). This absorption band can be assigned to the $S_0 \rightarrow S_1$ transition and attributed to two electronic transitions: HOMO → LUMO (87%) and HOMO−1 → LUMO+1 (13%). The theoretical value is in very good agreement with the experimental absorption value (λ_{exp} = 420 nm), thus confirming the existence of the bis-keto form in solution.

3.7. Al_2-Vm_2 complex

We have optimized the Al^{3+} complex with the **H_2Vm** ligand using M : L = 1 : 1 stoichiometry since it has been evidenced experimentally by the Job's plot analysis. The minimum energy geometry (considering a dinuclear system) is shown in Fig. 7, where each metal center is coordinated to two phenoxide O atoms and two N atoms of the imine bonds. Each Al^{3+} is also coordinated to one nitrato ligand, thus yielding a neutral dinuclear complex.

To provide reliability for the geometry proposed above, we also performed a TD-DFT study of the complex. In the ground state (S_0) of the Al^{3+} complex the HOMO and HOMO−1 are composed of two phenolic aromatic moieties of the ligands and the conjugated C=N bonds (Fig. 8a and 9). Interestingly, the LUMO and LUMO+2 are composed of the nitrato ligand with some contribution from the antibonding C=N π orbital. In contrast, the atomic orbitals of the nitrato ligand do not contribute to the LUMO+1. The energy difference between the HOMO and LUMO is 3.510 eV. To get better insight into the experimental absorption values, TDDFT calculations were per-

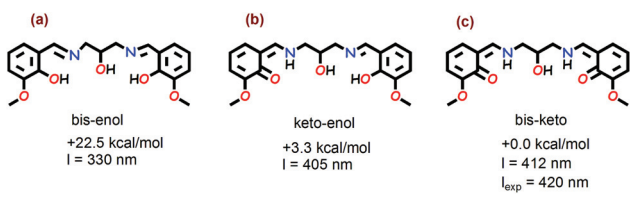

Scheme 2 Keto–enol equilibrium of the ligand, energetic differences at the B3LYP/6-311+G* level of theory and theoretical lowest energy lying absorption band.

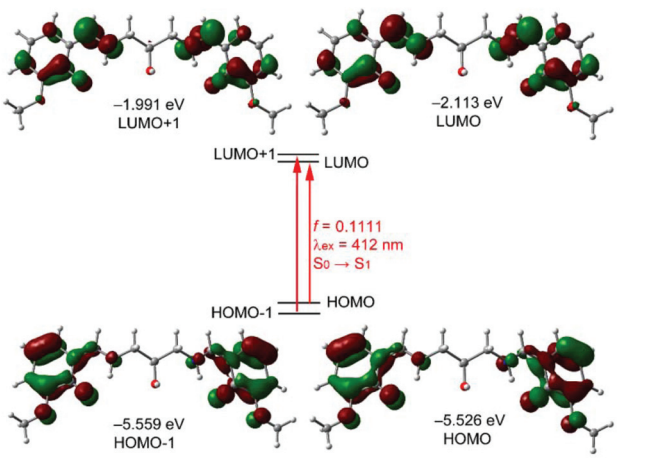

Fig. 6 Molecular orbitals involved in the UV-vis absorption of the bis-keto form of the ligand at the B3LYP/6-311+G* level of theory.

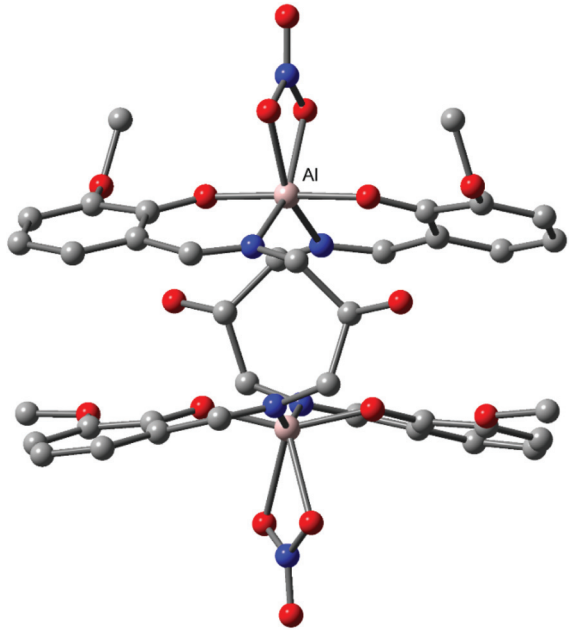

Fig. 7 B3LYP/6-311+G* optimized structure of the [Al_2-Vm_2] complex. H-Atoms omitted for clarity.

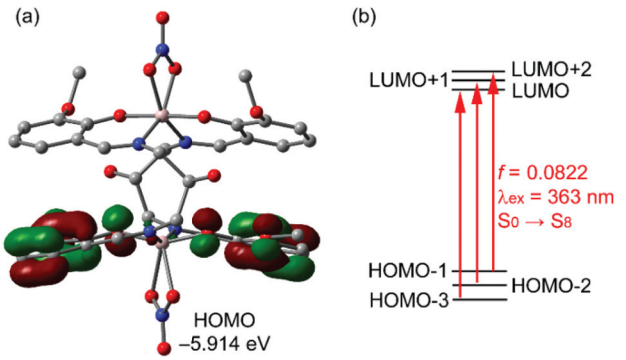

Fig. 8 (a) Plot of the HOMO and (b) frontier molecular orbitals involved in the lowest lying observable UV-vis absorption of the complex [Al_2-Vm_2 (NO_3)$_2$] at the B3LYP/6-311+G* level of theory.

formed for the complex on the basis of the optimized geometry. The calculated absorption energy associated with its oscillator strength, the main configurations and their assignments of the lowest-lying transition in the Al^{3+} complex are given in Table S5.† The singlet → singlet absorption band corresponds to the $S_0 \rightarrow S_8$ excitation (3.4147 eV, λ = 363 nm and f = 0.0822). This single excitation can be attributed to HOMO−3 → LUMO, HOMO−2 → LUMO+1 and HOMO−1 → LUMO+2 transitions (Fig. 8b), which can be assigned to π(L) → π*(L) transitions with ILCT character. The experimental value (λ_{exp} = 368 nm) is in very good agreement with the theoretical value (363 nm), thus giving reliability to the optimized complex shown in Fig. 7. The theoretical UV-vis spectrum is given in Fig. S29.†

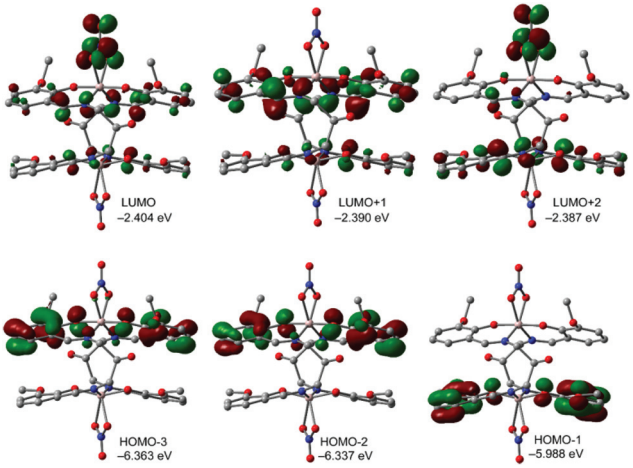

Fig. 9 Frontier molecular orbitals involved in the lowest lying observable UV-vis absorption of the complex [Al_2-Vm_2 (NO_3)$_2$] at the B3LYP/6-311+G* level of theory.

3.8. Al_2-Vm_2 complex with picric acid (2)

We have optimized the Al^{3+} complex using picric acid instead of nitrate, since it has been shown experimentally that Al^{3+} is able to recognize picric acid. The geometry of the optimized complex is shown in Fig. 10. It can be observed that the geometry is similar to that previously described for nitrate. The picric acid is coordinated to the metal center by means of the phenolate O atom.

3.9. Application of H_2Vm for Al^{3+} detection in live cells

The probe, **H_2Vm**, has a thermodynamically favourable binding affinity to $Al(NO_3)_3{\cdot}9H_2O$ and forms an **Al_2-Vm_2** complex, which gives an emission spectra in the visible range. Keeping this in mind it was conceived that the compound could be exploited for fluorescence imaging of live cells, particularly for the sensitive detection of intracellular Al^{3+}. However, to materialize this objective it is a prerequisite to assess the cytotoxicity of the probe, $Al(NO_3)_3{\cdot}9H_2O$ and the complex on live cells. The well-established MTT assay, which is based on the mitochondrial dehydrogenase activity of viable cells was adopted to study the cytotoxicity of the abovemen-

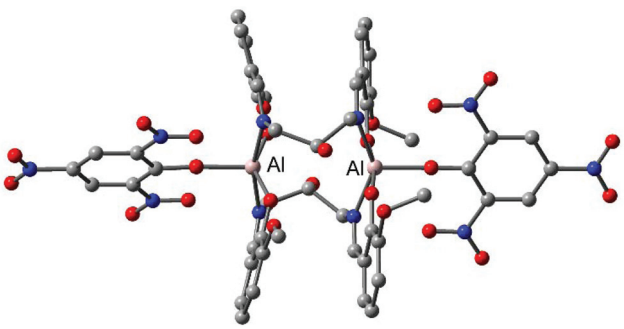

Fig. 10 B3LYP/6-311+G* optimized structure of the [Al_2-Vm_2PA_2] complex. H-Atoms omitted for clarity.

tioned compounds at varying concentrations, as mentioned in Methods section. Fig. S30† shows that the probe did not exert any adverse effects on cell viability at lower concentrations. Same was the case when the cells were treated with $Al(NO_3)_3{\cdot}9H_2O$ in lower concentrations. However, exposure of the HCT cells to the **Al_2-Vm_2** complex resulted in a decline in cell viability above a concentration of 20 μM. The effect was more pronounced in higher concentrations, and adverse cytotoxicity was observed in a dose-dependent manner. The observed cytotoxicity could be attributed to the **Al_2-Vm_2** complex formation. The results obtained in the *in vitro* cytotoxic assay suggested that in order to pursue fluorescence imaging studies of the **Al_2-Vm_2** complex in live cells, it would be prudent to choose a working concentration of 20 μM for the probe. Hence, to assess the effectiveness of a compound as a probe for intracellular detection of Al^{3+} by fluorescence microscopy, HCT cells were treated with 20 μM $Al(NO_3)_3{\cdot}9H_2O$ for 1 h, followed by a 10 μM probe solution to promote the formation of the **Al_2-Vm_2** complex. Fluorescence microscopic studies revealed no fluorescence in cells when treated with either the probe compound or $Al(NO_3)_3{\cdot}9H_2O$ alone (Fig. 11). Upon incubation with $Al(NO_3)_3{\cdot}9H_2O$, followed by the probe compound, a striking switch-on fluorescence was observed inside the cells, which indicated the formation of the **Al_2-Vm_2** complex, as observed earlier in solution studies (Fig. 11). Furthermore, an intense blue fluorescence was observed in the cytoplasmic region but not in the nucleus. The fluorescence microscopic analysis strongly suggested that the probe could readily cross the membrane barrier, permeate into the HCT cells, and rapidly sense intracellular Al^{3+}. It is significant to mention here that the bright field images of treated cells did not reveal any gross morphological changes, which suggested that the cells were viable. These findings open up the avenue for future *in vivo* biomedical applications of the sensor.

3.10. Application of Al_2-Vm_2 for picric acid detection in live cells

Fluorescent microscopic analysis was performed in the same way as mentioned above to detect picric acid. The HCT 116 cells were first treated with 20 μM $Al(NO_3)_3{\cdot}9H_2O$ for 1 h, followed by a 10 μM probe solution to promote the formation of the **Al_2-Vm_2** complex. This was followed by incubation with 20 μM of picric acid solution. The bright blue fluorescence of the cells containing the **Al_2-Vm_2** complex was no more visible probably due to the quenching action of PA. Only the nuclei were visible due to the nuclear stain DAPI (Fig. 12).

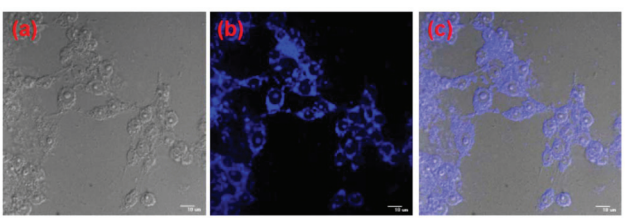

Fig. 11 Fluorescence confocal microscopic images of the probe **H_2Vm** and $Al(NO_3)_3{\cdot}9H_2O$ in HCT 116 cells. All images were acquired with a 40× objective lens. (a) Bright field image of the cells without any treatment. (b) Dark field image of the cells treated with the aluminium probe, **H_2Vm** (20 μM) and $Al(NO_3)_3{\cdot}9H_2O$ (20 μM), nuclei counterstained with DAPI (1 μg mL^{-1}). (c) Bright field image of the cells treated with the aluminium probe, H_2Vm (20 μM) and $Al(NO_3)_3{\cdot}9H_2O$ (20 μM).

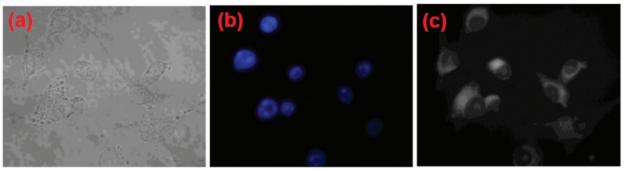

Fig. 12 Fluorescence confocal microscopic images of the probe **H_2Vm**, $Al(NO_3)_3{\cdot}9H_2O$ and picric acid (PA) in HCT 116 cells. All images were acquired with a 40× objective lens. (a) Bright field image of the cells without any treatment. (b) Dark field image of the cells treated with **H_2Vm** (20 μM), $Al(NO_3)_3{\cdot}9H_2O$ (20 μM) and picric acid (PA), nuclei counterstained with DAPI (1 μg mL^{-1}). (c) Bright field image of the cells treated with **H_2Vm** (20 μM), $Al(NO_3)_3{\cdot}9H_2O$ (20 μM) and picric acid (PA).

4. Conclusions

In conclusion, we have explored the probe, 6,6′-(1*E*,1′*E*)-(2-hydroxypropane-1,3-diyl)bis(azan-1-yl-1-ylidene)bis(methan-1-yl-1-ylidene)bis(2-methoxyphenol) (**H_2Vm**), as a "switch-on" chemosensor for Al^{3+}. The Al^{3+}-responsive behavior of the sensor was investigated by means of UV-Vis and fluorescence spectroscopic methods. The addition of Al^{3+} to **H_2Vm** triggers a significant switch-on fluorescence response and exhibits excellent selectivity toward Al^{3+} with no apparent interference from other relevant cations, indicating that the Al^{3+}-induced fluorescence response can coexist in common metal ions. The sensing mechanism can be ascribed to the chelation-enhanced fluorescence (CHEF) process. The composition of the **Al_2-Vm_2** aggregate was determined by means of ^{1}H and ^{13}C-NMR experiments. Strikingly, the **Al_2-Vm_2** ensemble produces a "switch-off" fluorescence response for the well-known explosive picric acid. Detailed theoretical investigations were performed for **H_2Vm**, the **Al_2-Vm_2** aggregate and the complex between **Al_2-Vm_2** and picric acid. Furthermore, we demonstrated the effective sensing of Al^{3+} by **H_2Vm** and PA by the **Al_2-Vm_2** ensemble in HCT 116 live cells.

Conflicts of interest

There are no conflicts to declare.

Acknowledgements

B. Naskar acknowledges University Grants Commission, India for fellowship (Sanction No. RGNF-2013-14-SC-WES-38844). A. B. and A. F. thank MINECO/AEI of Spain (projects CTQ2014-57393-C2-1-P and CTQ2017-85821-R,

FEDER funds) for funding. We are grateful to the CTI (UIB) for free allocation of computer time.

Notes and references

1 (*a*) D. Wu, A. C. Sedgwick, T. Gunnlaugsson, E. U. Akkaya, J. Yoonand and T. D. James, *Chem. Soc. Rev.*, 2017, **46**, 7105–7123; (*b*) L. He, B. Dong, Y. Liuand and W. Lin, *Chem. Soc. Rev.*, 2016, **45**, 6449–6461; (*c*) A. Gupta and N. Kumar, *RSC Adv.*, 2016, **6**, 106413–106434; (*d*) M. Saleem and K. H. Lee, *RSC Adv.*, 2015, **5**, 72150–72287; (*e*) W. H. Ding, W. Cao, X. J. Zheng, D. C. Fang, W. T. Wong and L. P. Jin, *Inorg. Chem.*, 2013, **52**, 7320–7322.

2 (*a*) D. Maity and T. Govindaraju, *Eur. J. Inorg. Chem.*, 2011, **2011**, 5479–5485; (*b*) S. Pu, C. Zhang, C. Fan and G. Liu, *Dyes Pigm.*, 2016, **129**, 24–33.

3 (*a*) G. D. Fasman, *Coord. Chem. Rev.*, 1996, **149**, 125; (*b*) T. P. Flaten, *Brain Res. Bull.*, 2001, **55**, 187; (*c*) J. R. Walton, *Neurotoxicology*, 2006, **27**, 385; (*d*) B. R. Stephens and J. S. Jolliff, *Diet and Nutrition in Dementia and Cognitive Decline*, 2015, pp. 553–562; (*e*) P. Nayak, *Environ. Res.*, 2002, **89**, 101–115; (*f*) D. Sarkar, P. Ghosh, S. Gharami, T. K. Mondal and N. Murmu, *Sens. Actuators, B*, 2017, **242**, 338–346; (*g*) J. Jun Lee, G. J. Park, Y. S. Kim, S. Y. Lee, H. J. Lee, I. S. Noh and C. Kim, *Biosens. Bioelectron.*, 2015, **69**, 226–229; (*h*) Y. W. Choi, G. J. Park, Y. J. Na, H. Y. Jo, S. A. Lee, G. R. You and C. Kim, *Sens. Actuators, B*, 2014, **194**, 343–352.

4 A. Tong, Y. Akama and S. Tanaka, *Analyst*, 1990, **115**, 947–949.

5 G. P. C. Rao, K. Seshaiah, Y. K. Rao and M. C. Wang, *J. Agric. Food Chem.*, 2006, **54**, 2868–2872.

6 *Aluminium in drinking-water: Background document for development of WHO Guidelines for Drinking-water Quality*, World Health Organization, 2010, WHO Reference number: WHO/HSE/WSH/10.01/13.

7 (*a*) K. Soroka, R. S. Vithanage, D. A. Phillips, B. Walker and P. K. Dasgupta, *Anal. Chem.*, 1987, **59**, 629; (*b*) V. Kumar, P. Kumar and R. Gupta, *RSC Adv.*, 2017, **7**, 23127–23135.

8 (*a*) X. Sun, Y. Wang and Y. Lei, *Chem. Soc. Rev.*, 2015, **44**, 8019–8061; (*b*) Y. Salinas, R. Martinez-Manez, M. D. Marcos, F. Sancenon, A. M. Costero, M. Parra and S. Gil, *Chem. Soc. Rev.*, 2012, **41**, 1261–1296; (*c*) G. V. Zyryanov, D. S. Kopchuk, I. S. Kovalev, E. V. Nosova, V. L. Rusinov and O. N. Chupakhin, *Russ. Chem. Rev.*, 2014, **83**, 783; (*d*) R. G. Smith, N. D. Souza and S. Nicklin, *Analyst*, 2008, **133**, 571–584; (*e*) N. Sang, C. Zhan and D. Cao, *J. Mater. Chem. A*, 2015, **3**, 92–96; (*f*) K. S. Asha, G. S. Vaisakhan and S. Mandal, *Nanoscale*, 2016, **8**, 11782–11786.

9 S. S. Nagarkar, A. V. Desai and S. K. Ghosh, *CrystEngComm*, 2016, **18**, 2994–3007.

10 (*a*) C. Beyer, U. Bohme, C. Pietzsch and G. Roewer, *J. Organomet. Chem.*, 2002, **654**, 187–201; (*b*) E. Bingham, B. Cohrssen and C. H. Powell, *Patty's, Toxicology*, John Wiley& Sons, New York, 2000, vol. IIB, p. 980; (*c*) S. Singh, *J. Hazard. Mater.*, 2007, **144**, 15–28; (*d*) S. Talmage, D. Opresko, C. Maxwell, C. E. Welsh, F. M. Cretella, P. Reno and F. B. Daniel, in *Rev. Environ. Contam T*, ed. G. Ware, Springer, New York, 1999, vol. 161, pp. 1–156; (*e*) S. Barman, J. Anand Garg, O. Blacque, K. Venkatesan and H. Berke, *Chem. Commun.*, 2012, **48**, 11127–11129; (*f*) T. L. Davis, *The Chemistry of Powder and Explosives*, Angriff Press, 1943.

11 (*a*) L. Zhang, Z. Kang, X. Xin and D. Sun, *CrystEngComm*, 2016, **18**, 193–206; (*b*) Q. H. Tan, Y. Q. Wang, X. Y. Guo, H. T. Liu and Z. L. Liu, *RSC Adv.*, 2016, **6**, 61725–61731; (*c*) R. B. Fu, S. M. Hu and X. T. Wu, *Cryst. Growth Des.*, 2016, **16**, 5074–5083.

12 (*a*) Environmental Protection Agency, innovative treatment technologies: Annual status report, 8th edn, 1996, EPA-542-R-96-010; (*b*) Y. H. Lee, H. Liu, J. Y. Lee, S. H. Kim, S. K. Kim, J. L. Sessler, Y. Kim and J. S. Kim, *Chem. – Eur. J.*, 2010, **16**, 5895–5901.

13 (*a*) S. Shanmugaraju, S. A. Joshi and P. S. Mukherjee, *J. Mater. Chem.*, 2011, **21**, 9130–9138; (*b*) M. E. Germain and M. J. Knapp, *Chem. Soc. Rev.*, 2009, **38**, 2543–2555; (*c*) K. K. Kartha, A. Sandeep, V. K. Praveen and A. Ajayaghosh, *Chem. Rec.*, 2015, **15**, 252–265; (*d*) S. Shanmugaraju, H. Jadhav and P. Mukherjee, *Proc. Natl. Acad. Sci., India, Sect. A*, 2014, **84**, 197–203; (*e*) H. T. Feng and Y. S. Zheng, *Chem. – Eur. J.*, 2014, **20**, 195–201.

14 (*a*) M. A. Ivy, L. T. Gallagher, A. D. Ellington and E. V. Anslyn, *Chem. Sci.*, 2012, **3**, 1773–1779; (*b*) A. Buragohain, M. Yousufuddin, M. Sarma and S. Biswas, *Cryst. Growth Des.*, 2016, **16**, 842–851; (*c*) M. Sk and S. Biswas, *CrystEngComm*, 2016, **18**, 3104–3113; (*d*) S. S. Nagarkar, A. V. Desai and S. K. Ghosh, *Chem. Commun.*, 2014, **50**, 8915–8918; (*e*) X. H. Zhou, L. Li, H. H. Li, A. Li, T. Yang and W. Huang, *Dalton Trans.*, 2013, **42**, 12403–12409; (*f*) S. S. Nagarkar, A. V. Desai, P. Samanta and S. K. Ghosh, *Dalton Trans.*, 2015, **44**, 15175–15180; (*g*) S. S. Nagarkar, B. Joarder, A. K. Chaudhari, S. Mukherjee and S. K. Ghosh, *Angew. Chem., Int. Ed.*, 2013, **52**, 2881–2885; (*h*) B. Joarder, A. V. Desai, P. Samanta, S. Mukherjee and S. K. Ghosh, *Chem. – Eur. J.*, 2014, **20**, 1–6; (*i*) X. Z. Song, S. Y. Song, S. N. Zhao, Z. M. Hao, M. Zhu, X. Meng, L. L. Wu and H. J. Zhang, *Adv. Funct. Mater.*, 2014, **24**, 4034–4041; (*j*) T. Wen, D. X. Zhang, J. Liu, R. Lin and J. Zhang, *Chem. Commun.*, 2013, **49**, 5660–5662; (*k*) L. Zhao, J. Ye, W. Li, R. F. Bogale, B. Wang, W. Gong and G. Ning, *Inorg. Chem. Commun.*, 2014, **46**, 212–215; (*l*) J. D. Xiao, L. G. Qiu, F. Ke, Y. P. Yuan, G. S. Xu, Y. M. Wang and X. Jiang, *J. Mater. Chem. A*, 2013, **1**, 8745–8752; (*m*) S. Mukherjee, A. V. Desai, B. Manna, A. I. Inamdar and S. K. Ghosh, *Cryst. Growth Des.*, 2015, **15**, 4627–4634.

15 (*a*) D. S. Moore, *Rev. Sci. Instrum.*, 2004, **75**, 2499–2512; (*b*) J. M. Sylvia, J. A. Janni, J. D. Klein and K. M. Spencer, *Anal. Chem.*, 2000, **72**, 5834–5840; (*c*) J. A. Caulfield, T. J. Bruno and K. E. Miller, *J. Chem. Eng. Data*, 2009, **54**,

1814–1822; (*d*) K. H°akansson, R. V. Coorey, R. A. Zubarev, V. L. Talrose and P. H°akansson, *J. Mass Spectrom.*, 2000, **35**, 337–346; (*e*) R. D. Luggar, M. J. Farquharson, J. A. Horrocks and R. J. Lacey, *X-Ray Spectrom.*, 1998, **27**, 87–94; (*f*) V. P. Anferov, G. V. Mozjoukhineand and R. Fisher, *Rev. Sci. Instrum.*, 2000, **71**, 1656–1659; (*g*) H. Chen, B. Dong, Y. Tang and W. Lin, *Acc. Chem. Res.*, 2017, **50**, 1410–1422; (*h*) L. He, B. Dong, Y. Liu and W. Lin, *Chem. Soc. Rev.*, 2016, **45**, 6449–6461; (*i*) Y. Tang, D. Lee, J. Wang, G. Li, J. Yu, W. Lin and J. Yoon, *Chem. Soc. Rev.*, 2015, **44**, 5003–5015.

16 (*a*) S. Madhu, A. Bandela and M. Ravikanth, *RSC Adv.*, 2014, **4**, 7120–7123; (*b*) X. Sun, Y. Wang and Y. Lei, *Chem. Soc. Rev.*, 2015, **44**, 8019; (*c*) V. Bereau, C. Duhayon and J. P. Sutter, *Chem. Commun.*, 2014, **50**, 12061–12064; (*d*) K. Maiti, A. K. Mahapatra, A. Gangopadhyay, R. Maji, S. Mondal, S. S. Ali, S. Das, R. Sarkar, P. Datta and D. Mandal, *ACS Omega*, 2017, **2**, 1583–1593; (*e*) S. Maity, M. Shyamal, D. Das, P. Mazumdar, G. P. Sahoo and A. Misra, *Sens. Actuators, B*, 2017, **248**, 223–233; (*f*) R. Sodkhomkhum, M. Masik, S. Watchasit, C. Suksai, J. Boonmak, S. Youngme, N. Wanichacheva and V. Ervithayasuporn, *Sens. Actuators, B*, 2017, **245**, 665–673; (*g*) S. Kumari, S. Joshi, T. C. Cordova-Sintiago, D. D. Pant and R. Sakhuja, *Sens. Actuators, B*, 2016, **229**, 599–608.

17 (*a*) Y. Fang, Y. Zhou, Q. Rui and C. Yao, *Organometallics*, 2015, **34**, 2962–2970; (*b*) Y. Zhang, D. Li, Y. Li and J. Yu, *Chem. Sci.*, 2014, **5**, 2710–2716.

18 (*a*) M. Dolai, T. Mistri, A. Panja and M. Ali, *Inorg. Chim. Acta*, 2013, **399**, 95–104; (*b*) M. Dolai, M. Ali, J. Titiš and R. Boča, *Dalton Trans.*, 2015, **44**, 13242–13249; (*c*) S. Liao, X. Yang and R. A. Jones, *Cryst. Growth Des.*, 2012, **12**, 970–974; (*d*) K. Griffiths, J. Mayans, M. A. Shipman, G. J. Tizzard, S. J. Coles, B. A. Blight, A. Escuerand and G. E. Kostakis, *Cryst. Growth Des.*, 2017, **17**, 1524–1538; (*e*) G. Fu, B. Li, J. Guo, L. Liu, K. Zhang, W. Feng and X. Lü, *Cryst. Growth Des.*, 2018, **18**, 1020–1029; (*f*) L. Jiang, D. Y. Zhang, J. J. Suo, W. Gu, J. L. Tian, X. Liu and S. P. Yana, *Dalton Trans.*, 2016, **45**, 10233–10248; (*g*) L. Jiang, Y. Liu, X. Liu, J. Tian and S. Yan, *Dalton Trans.*, 2017, **46**, 12558–12573; (*h*) V. Chandrasekhar, A. Dey, S. Das, M. Rouzieres and R. Clerac, *Inorg. Chem.*, 2013, **52**, 2588–2598; (*i*) K. I. Smith, L. L. Borer and M. M. Olmstead, *Inorg. Chem.*, 2003, **42**, 7410–7415; (*j*) A. Dey, S. Das, S. Kundu, A. Mondal, M. Rouzieres, C. Mathoniere, R. Clerac, R. S. Narayananand and V. Chandrasekhar, *Inorg. Chem.*, 2017, **56**, 14612–14623; (*k*) A. Datta, J. K. Clegg, J. H. Huang, A. Pevec, E. Garribba and M. Fondo, *Inorg. Chem. Commun.*, 2012, **24**, 216–220; (*l*) S. R. Doctrow, K. Huffman, C. B. Marcus, G. Tocco, E. Malfroy, C. A. Adinolfi, H. Kruk, K. Baker, N. Lazarowych, J. Mascarenhas and B. Malfroy, *J. Med. Chem.*, 2002, **4**(5), 4549–4558; (*m*) A. Elmali, C. T. Zeyrek and Y. Elerman, *J. Mol. Struct.*, 2004, **693**, 225–234; (*n*) P. M. Anarjan, R. Bikas, H. H. Monfared, P. Aleshkevych and P. Mayer, *J. Mol. Struct.*, 2017, **1131**, 258–265; (*o*) L. Paul, B. Banerjee, A. Bhaumik and M. Ali, *Microporous Mesoporous Mater.*, 2017, **249**, 78–87; (*p*) M. Mitra, A. K. Maji, B. K. Ghosh, P. Raghavaiah, J. Ribas and R. Ghosh, *Polyhedron*, 2014, **67**, 19–26; (*q*) S. Pal, B. Chowdhury, M. Patra, M. Maji and B. Biswas, *Spectrochim. Acta, Part A*, 2015, **144**, 148–154; (*r*) B. N. Ghose, *Synth. React. Inorg. Met.-Org. Chem.*, 1982, **12**, 835–843; (*s*) A. Dey, S. Das, M. A. Palacios, E. Colacio and V. Chandrasekhar, *Eur. J. Inorg. Chem.*, 2018, **15**, 1645–1654.

19 (*a*) M. E. Casida, C. Jamoroski, K. C. Casida and D. R. Salahub, *J. Chem. Phys.*, 1998, **108**, 4439–4449; (*b*) R. E. Stratmann, G. E. Scuseria and M. J. Frisch, *J. Chem. Phys.*, 1998, **109**, 8218–8224; (*c*) R. Bauernschmitt and R. Ahlrichs, *Chem. Phys. Lett.*, 1996, **256**, 454–464.

20 J. P. Perdew, *Phys. Rev. B: Condens. Matter Mater. Phys.*, 1986, **33**, 8822–8824.

21 (*a*) M. Cossi, N. Rega, G. Scalmani and V. Barone, *J. Comput. Chem.*, 2003, **24**, 669–681; (*b*) M. Cossi and V. Barone, *J. Chem. Phys.*, 2001, **115**, 4708–4717; (*c*) V. Barone and M. Cossi, *J. Phys. Chem. A*, 1998, **102**, 1995–2001.

22 M. J. Frisch, G. W. Trucks, H. B. Schlegel, G. E. Scuseria, M. A. Robb, J. R. Cheeseman, G. Scalmani, V. Barone, B. Mennucci, G. A. Petersson, H. Nakatsuji, M. Caricato, X. Li, H. P. Hratchian, A. F. Izmaylov, J. Bloino, G. Zheng, J. L. Sonnenberg, M. Hada, M. Ehara, K. Toyota, R. Fukuda, J. Hasegawa, M. Ishida, T. Nakajima, Y. Honda, O. Kitao, H. Nakai, T. Vreven, J. A. Montgomery Jr., J. E. Peralta, F. Ogliaro, M. Bearpark, J. J. Heyd, E. Brothers, K. N. Kudin, V. N. Staroverov, R. Kobayashi, J. Normand, K. Raghavachari, A. Rendell, J. C. Burant, S. S. Iyengar, J. Tomasi, M. Cossi, N. Rega, J. M. Millam, M. Klene, J. E. Knox, J. B. Cross, V. Bakken, C. Adamo, J. Jaramillo, R. Gomperts, R. E. Stratmann, O. Yazyev, A. J. Austin, R. Cammi, C. Pomelli, J. W. Ochterski, R. L. Martin, K. Morokuma, V. G. Zakrzewski, G. A. Voth, P. Salvador, J. J. Dannenberg, S. Dapprich, A. D. Daniels, Ö. Farkas, J. B. Foresman, J. V. Ortiz, J. Cioslowski and D. J. Fox, *GAUSSIAN 09 (Revision C.01)*, Gaussian, Inc., Wallingford, CT, 2009.

23 (*a*) H. A. Benesi and J. H. Hildebrand, *J. Am. Chem. Soc.*, 1949, **71**, 2703–2707; (*b*) S. Sinha, B. Chowdhury and P. Ghosh, *Inorg. Chem.*, 2016, **55**, 9212–9220.

24 (*a*) J. R. Walton, *Neurotoxicology*, 2006, **27**, 385; (*b*) S. Das, A. Sahana, A. Banerjee, S. Lohar, D. A. Safin, M. G. Babashkina, M. Bolte, Y. Garcia, I. Hauli, S. K. Mukhopadhyay and D. Das, *Dalton Trans.*, 2013, **42**, 4757–4763.

25 J. R. Lakowicz, *Priniples of Fluorescence Spectroscopy*, Plenum, New York, 3rd edn, 2006.

